THE JOURNAL OF PHYSICAL CHEMISTRY Letters

Letter

Cite This: J. Phys. Chem. Lett. 2018, 9, 4287−4293

pubs.acs.org/JPCL

Membrane Charging and Swelling upon Calcium Adsorption as Revealed by Phospholipid Nanodiscs

Orion Shih,[†] Yi-Qi Yeh,[†] Kuei-Fen Liao,[†] Chun-Jen Su,[†] Pei-Hao Wu,[‡] Richard K. Heenan,[§] Tsyr-Yan Yu,*[,‡] and U-Ser Jeng*[,†,∥]

[†]National Synchrotron Radiation Research Center, Hsinchu 30076, Taiwan

[‡]Institute of Atomic and Molecular Sciences, Academia Sinica, Taipei 10617, Taiwan

[§]STFC ISIS Facility, Rutherford-Appleton Laboratory, Building R3, Didcot, OX11 0QX, U.K.

[∥]Department of Chemical Engineering, National Tsing Hua University, Hsinchu 30013, Taiwan

Supporting Information

ABSTRACT: Direct binding of calcium ions (Ca^{2+}) to phospholipid membranes is an unclarified yet critical signaling pathway in diverse Ca^{2+}-regulated cellular phenomena. Here, high-pressure-liquid-chromatography, small-angle X-ray scattering (SAXS), UV−vis absorption, and differential refractive index detections are integrated to probe Ca^{2+}-binding to the zwitterionic lipid membranes in nanodiscs. The responses of the membranes upon Ca^{2+}-binding, in composition and conformation, are quantified through integrated data analysis. The results indicate that Ca^{2+} binds specifically into the phospholipid headgroup zone, resulting in membrane charging and membrane swelling, with a saturated Ca^{2+}-lipid binding ratio of 1:8. A Ca^{2+}-binding isotherm to the nanodisc is further established and yields an unexpectedly high binding constant K = 4260 M^{-1} and a leaflet potential of ca. 100 mV based on a modified Gouy−Chapman model. The calcium-lipid binding ratio, however, drops to 40% when the nanodisc undergoes a gel-to-fluid phase transition, leading to an effective charge capacity of a few $\mu F/cm^2$.

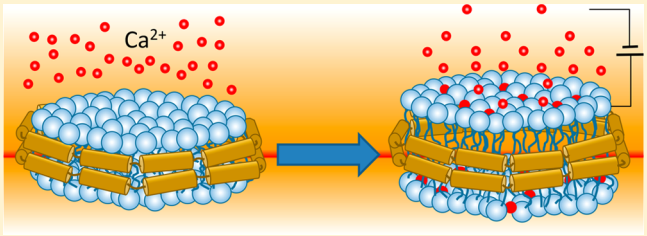

Calcium ions (Ca^{2+}) play important roles in many cellular processes. As a well-known secondary messenger, Ca^{2+} regulates diverse signaling processes through interactions with membrane proteins or directly with cellular membranes, which is a crucial factor for the transportation of small molecules across membranes (endo- or exocytosis).[1−3] Up to date, the corresponding mechanisms and pathways of these Ca^{2+}-involved biological processes await to be resolved. Especially, how membranes respond to direct Ca^{2+} adsorption still remains elusive.[4,5] Part of the difficulties arise from the lack of a well-defined membrane platform and no single tool sensitive enough for elucidating the delicate structural and compositional changes in membranes upon calcium adsorption. Previously, phospholipid vesicle bilayers were commonly adopted as model membranes for studies of calcium-membrane interactions using X-ray diffraction,[6−9] NMR,[10−12] isothermal titration calorimetry,[13−15] infrared spectroscopy,[16] dynamic light scattering,[17,18] ζ-potential measurements,[19−21] particle electrophoresis,[10,19,21] or small-angle neutron scattering.[22] Nevertheless, the instability of vesicle membranes toward environmental stimulations and high polydispersity in size and curvature resulted in scattered or inconsistent experimental results. For example, the intrinsic binding constant of calcium to phosphatidylcholine estimated in previous studies[6,12,20,23] scatter between 0.1 and 100 M^{-1}.

Recently, the fast-growing nanodisc technology provides stable and highly monodisperse model membranes for structural and functional characterizations of membrane proteins.[24] Nanodiscs are discoidal phospholipid bilayers laterally surrounded and stabilized by membrane scaffold protein (MSP) belts. It consists of a lipid bilayer of 100−300 phospholipids,[25,26] depending on the lipid type and the sequence of amphipathic MSPs. Previous studies have demonstrated that membrane proteins can be incorporated into the phospholipid bilayer of nanodiscs for functional and structural studies.[24,27,28] Compared to conventional vesicle bilayers, the planar and smaller lipid bilayers in nanodiscs are much more stable and monodisperse in size, allowing observation of structural changes with reduced complexity in structural analysis. Using nanodiscs to probe the small structural changes of membranes upon calcium binding, however, requires a set of integrated structural probes that provide complementary information to unveil the compositional and small structural changes in the multicomponent nanodisc complex. Owing to their great flexibility in tuning the lipid composition and membrane sizes for accommodating specific membrane proteins, nanodiscs attract accelerating

Received: May 28, 2018
Accepted: July 12, 2018
Published: July 12, 2018

Downloaded via SYNCHROTRON RADIATION RESEARCH on January 21, 2019 at 03:24:16 (UTC).
See https://pubs.acs.org/sharingguidelines for options on how to legitimately share published articles.

© 2018 American Chemical Society

DOI: 10.1021/acs.jpclett.8b01651
J. Phys. Chem. Lett. 2018, 9, 4287−4293

applications in structural and functional studies of membrane proteins for, such as, therapeutic delivery and controlled immune responses. Developing integrated methods to characterize systematically nanodisc complexes plays a pivot role to catch up the research and industrial opportunities enabled by the nanodisc technology.[26]

In this study, we use MSP1D1(−)-dimyristoylphosphatidylcholine (DMPC) nanodiscs as a model membrane system and present a unique approach to probe quantitatively the membrane compositional and structural changes upon calcium adsorption. Specifically, high-pressure liquid chromatography (HPLC), small-angle X-ray scattering, UV−vis absorption, and differential refractive index (HPLC/SAXS/UV−vis/RI) are integrated to provide full-scope measurements for nanodiscs in calcium solution. Previous reports have already shown that online size exclusion column combined with SAXS enables SAXS data collection from a highly monodisperse species separated along the elution path.[29−31] Extracting relative structural changes in angstrom level for protein, nanodiscs, and protein-incorporated nanodiscs in solution[32,33] have been demonstrated to be feasible with SAXS.[34−36] With our newly developed integrated analysis scheme for calcium-nanodisc complex, the calcium-lipid binding ratio as well as the nanodisc composition can be model-independently determined from the absolute intensities of UV−vis absorption, SAXS, and RI signal measured from one sample elution of HPLC. Moreover, SAXS data collected using the online size-exclusion column ensures high sample monodispersity, which plays a critical role in revealing small membrane structural changes upon calcium adsorption. We further establish a binding isotherm of calcium to the nanodisc from the Ca-concentration dependent binding behavior, and extract a high binding affinity on the basis of a modified Gouy−Chapman model for electric double layers. The high Ca^{2+}-binding affinity and capacity to the nanodisc suggest that Ca^{2+}-membrane interaction is capable of affecting the regulation of calcium-dependent cellular processes.[5,37,38]

The numbers of the adsorbed Ca^{2+} (N_c) and lipids (N_l) in one nanodisc, as well as the number density of the nanodisc-Ca^{2+} complex (n_0) of the sample running through the HPLC/SAXS/UV−vis/RI system established (Figure S-1a), can be determined model-independently by correlating the RI signal (I_{RI}), UV−vis absorption intensity (I_{UV}), and the absolute zero-angle intensity of SAXS ($I_{o\text{-}SAXS}$) in a set of three equations

$$I_{RI} = C\left[\varphi_p\left(\frac{dn}{dc}\right)_p + \varphi_c\left(\frac{dn}{dc}\right)_c + (1-\varphi_p-\varphi_c)\left(\frac{dn}{dc}\right)_l\right] \quad (1)$$

$$I_{UV} = C\varphi_p\varepsilon L \quad (2)$$

$$I_{o\text{-}SAXS} = n_o(f_t - \rho_w V_t)^2 \quad (3)$$

where φ_p and φ_c correspond, respectively, to the mass fractions of protein and calcium ions within the complex, and $(dn/dc)_p$, $(dn/dc)_c$, and $(dn/dc)_l$ represent the RI increment for the protein, calcium ion, and lipid molecules. In eq 1, the (dn/dc) values can be found from literatures or approximated as detailed in the Supporting Information. In eq 2, I_{UV} at wavelength of 280 nm is contributed solely by MSP in our case, with the weight concentration of the nanodisc−Ca^{2+} complex C, extinction coefficient ε and path length L in the flow cell. In eq 3, $n_o = CN_A/M_t$, where N_A is the Avogadro's number and M_t is the molecular weight of the complex; ρ_w is the scattering length density (SLD) of the buffer. The total scattering length f_t and volume V_t of the Ca^{2+}-nanodisc complex are defined as summation from all contributed components. With eqs 1−3, n_o, φ_p, and φ_c can be resolved analytically in terms of the three absolute quantities I_{UV}, I_{RI}, and $I_{o\text{-}SAXS}$, measured for the three-component system of calcium-nanodisc complex (as expressed in eqs S-7 and S-8). Therefore, the numbers of lipids and bound calcium in the nanodisc $N_l = (1-\varphi_c-\varphi_p)M_pN_p/(\varphi_pM_l)$ and $N_c = \varphi_cM_pN_p/(\varphi_pM_c)$ can be uniquely determined (cf., the Supporting Information (SI) spreadsheet), with M_p, M_c, and M_l corresponding to the molecular weight of the protein, calcium, and lipid, respectively; N_p is the number of proteins in the complex and equals to two in this case.[26]

Figure 1 shows the profiles of $I_{o\text{-}SAXS}$, I_{UV}, and I_{RI} measured over the HPLC sample elution of the DMPC nanodiscs with

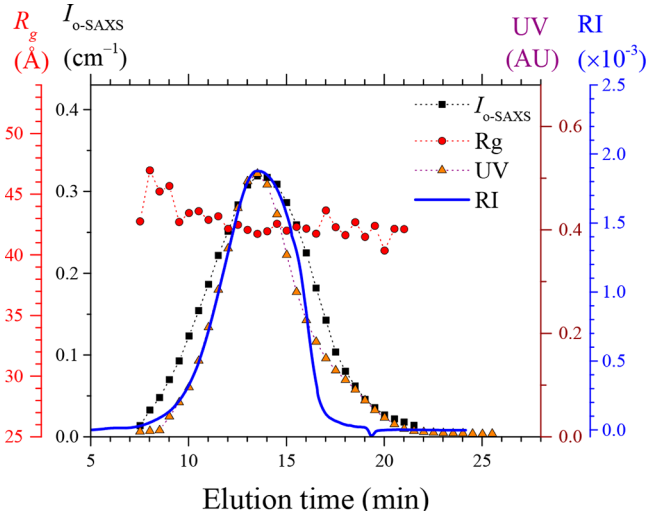

Figure 1. Profiles of I_{UV}, I_{RI}, $I_{o\text{-}SAXS}$, and R_g extracted from the HPLC/SAXS/UV−vis/RI data of the DMPC nanodisc with 25 mM $CaCl_2$. The three sets of data were measured along one sample elution path at 13 °C. The UV absorption signal at 280 nm and SAXS data were measured at the same sample position. The RI profile was measured at a later sample position, but is corrected to retrieve the peak profile (as shown) at the sample position of I_{UV} and $I_{o\text{-}SAXS}$, via a calibration measurement with cytochrome c.

25 mM $CaCl_2$. Also shown is the profile of the radius of gyration (R_g) extracted from the corresponding SAXS data using the Guinier approximation,[39] demonstrating a highly monodisperse R_g = 43.9 ± 0.1 Å of the Ca^{2+}−nanodisc complex over the major elution peak. From the peak values of the three overlapped profiles of $I_{o\text{-}SAXS}$, I_{UV}, and I_{RI}, and eqs 1−3, N_l = 178 and N_c = 18.8 are deduced model-independently. This yields a substantial calcium-lipid binding with a ratio χ_b (= N_c/N_l) of 0.106 in the medium size nanodisc with 89 lipids in each leaflet of the bilayer. Similarly, the compositions of the Ca^{2+}−nanodisc complex in 50 and 75 mM of $CaCl_2$ are determined. The results organized in Table 1 reveal that χ_b increases with the calcium concentration in solution, and saturates to χ_b = 0.12 at 75 mM $CaCl_2$, corresponding to a calcium/lipid binding ratio of 1:8 for the Ca^{2+}−nanodisc complex. Such calcium binding ratio with the zwitterionic lipid is reasonably smaller than the binding ratio 1:2 for calcium ions binding onto charged phosphatidylserine lipids in vesicles reported previously.[17] The N_l value (163) for

DOI: 10.1021/acs.jpclett.8b01651
J. Phys. Chem. Lett. 2018, 9, 4287−4293

Table 1. Absolute Peak Intensities I_{RI}, I_{UV}, and $I_{o\text{-}SAXS}$ Measured for the DMPC Nanodisc with Different [$CaCl_2$] Present in Buffer at 13 °C[a]

[$CaCl_2$]	0 mM	25 mM	50 mM	75 mM
I_{RI}	3.624×10^{-5}[b]	1.877×10^{-3}	2.193×10^{-3}	1.888×10^{-3}
I_{UV} (AU)	0.034[b]	0.509	0.608	0.547
$I_{0\text{-}SAXS}$ (cm^{-1})	0.320	0.320	0.373	0.317
R_g (Å)	43.9 ± 0.1	42.4 ± 0.1	42.2 ± 0.1	42.2 ± 0.1
N_l[c]	163 ± 18	178 ± 1	172 ± 1	161 ± 1
N_c		18.8 ± 8.4	20.0 ± 6.9	19.3 ± 7.4
χ_b		0.106 ± 0.047	0.117 ± 0.040	0.120 ± 0.046

[a]Calibrations of these absolute intensities are detailed in Figure S-1. R_g is the radius of gyration. N_c and N_l are numbers of Ca^{2+} and lipid in one nanodisc, and binding ratio χ_b is defined by N_c/N_l. [b]Taken from experiments using smaller sample volume with higher dilution factor compared to other conditions. [c]Uncertainties propagated from the absolute intensity calibrations are not included.

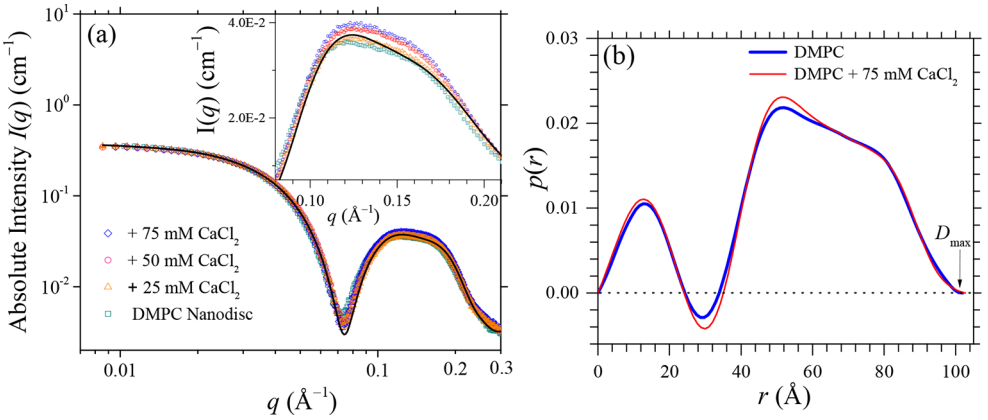

Figure 2. (a) SAXS data measured for the DMPC nanodisc in solutions of indicated $CaCl_2$ concentrations at 13 °C. Selectively shown is the fitting curve (black) for the data with 25 mM $CaCl_2$. Inset enlarges the details of the broad hump zone. (b) Corresponding distance distribution functions $p(r)$ Fourier transformed from the SAXS data, with a maximum distance D_{max} marked by an arrow.

the neat DMPC nanodisc derived from the integrated analysis agrees well with the number (162) estimated from calibrated M_w (154 kDa) of one nanodisc (Figure S-1c). Note that the small calcium ion adsorption contributes marginally to the change of nanodisc mass even with a saturated $\chi_b \approx 0.12$, corresponds to 0.8 kDa change (0.5%) in the M_w of the DMPC nanodisc, which is hard to be distinguished from the elution peak position change of the single-column HPLC system used. This fact highlights the sensitively of the integrated methodology developed here with HPLC/SAXS/UV−vis/RI. Previously, UV−vis and RI data were used to resolve the composition of a two-component system (protein-detergent complex) in solution.[29] Our further integration of SAXS into UV−vis/RI data analysis advances another critical step in the solution structure determination using the new nanodisc platform that involves three typical components: lipid, MSP, and accommodated membrane protein or adsorbed metallic ions.

To unveil the corresponding structural changes in the nanodisc upon the significant Ca^{2+} binding observed, we analyze the SAXS scattering profiles $I(q)$ as a function of the scattering vector $q = 4\pi\lambda^{-1}\sin\theta$, defined by the wavelength λ and scattering incident angle 2θ. As shown in Figure 2a, all the SAXS profiles of the DMPC nanodisc with [$CaCl_2$] ranging from 0 to 75 mM exhibit a broad hump centered around q = 0.12 $Å^{-1}$ (inset of Figure 2a), which corresponds to a characteristic size of ca. 50 Å for the discoidal shape of nanodiscs. The broad hump enhances in intensity as the $CaCl_2$ concentration increases. Correspondingly, the distance distribution function $p(r)$ calculated using GNOM[32] (Figure 2b) shows an enhanced $p(r)$ at $r \approx 50$ Å for the nanodisc with Ca^{2+} adsorption, compared to the SAXS data of the neat DMPC nanodisc. The negative-value zone near $r \approx 30$ Å exhibits a typical core−shell structure with a lower core SLD (lipid chain region) than that of the buffer and a higher SLD for the nanodisc shell (i.e., the MSP and the phosphocholine lipid heads). The maximum correlation length D_{max} for both cases are about the same (100 Å), indicating that overall size of the nanodisc is little affected by the Ca^{2+} adsorption. The demonstrated high monodispersity and stability of the nanodisc are crucial in the analysis of small changes in composition and structures of the nanodisc upon binding of small ions.

To extract the small structural changes revealed from the scattering data, we use an elliptical cylinder model (Figure 3a) to fit the full range of the SAXS data. In the model, the phospholipid bilayer is represented by a stack of elliptical cylinders with the core cylinder of bilayer lipid chains sandwiched by the top and bottom slabs of the lipid heads, and laterally surrounded with a shell of MSP. As representatively shown in Figure 2a, all features of the SAXS data for 25 mM $CaCl_2$ case could be adequately accounted by the model; all other sets of SAXS data could be fitted as well (detailed in Figure S-2b), using the parameters summarized in Table 2. The N_l values derived from the fitted nanodisc sizes and SLD for the nanodisc in solutions of 0, 25, 50, and 75 mM $CaCl_2$, match closely to those derived from the model-independent results shown in Table 1. Such consistency validates the reliability of the structural features revealed from the SAXS model-fitting, which include systemically increased

DOI: 10.1021/acs.jpclett.8b01651
J. Phys. Chem. Lett. 2018, 9, 4287−4293

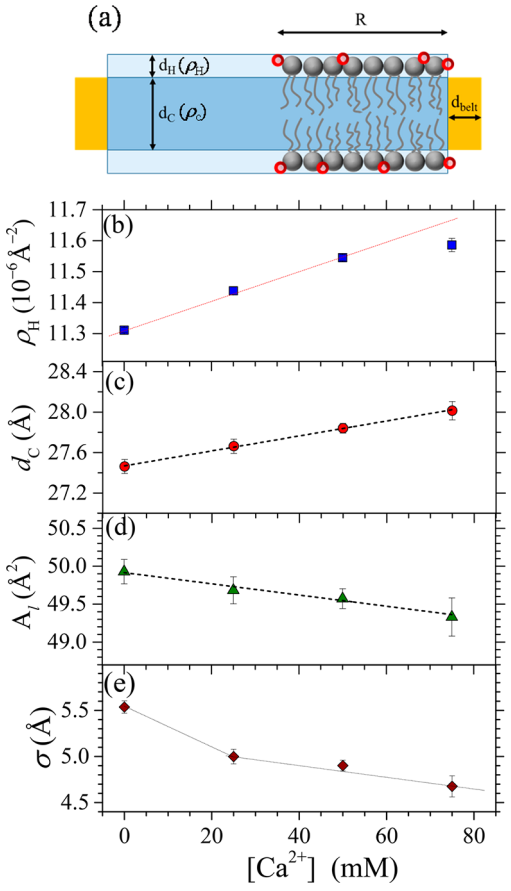

Figure 3. (a) Core−shell elliptical cylinder model for SAXS fitting of the Ca^{2+}-DMPC nanodisc complex, with core elliptical cylinder of semimajor and semiminor axes R and εR, core cylinder height d_C (with scattering length density ρ_C) for the bilayer hydrophobic alkyl chains, and the top and bottom discs with the same slab thickness d_H and scattering length density ρ_H for the hydrophilic lipid headgroup zone. The shell cylinder with thickness d_{belt} represents the two MSP that stabilize the nanodisc. Small circles in red are bound calcium ions. The interface roughness σ is not shown in the cartoon. Shown in panels b, c, and e are the critical structural parameters fitted for the $CaCl_2$-concentration dependent SAXS data shown in Figure 2. (d) Area per lipid A_l of DMPC molecules in the nanodisc, derived from the fitted parameters. The structural changes shown in panels c and d are fitted with linear regression lines.

SLD of the lipid head zone, ρ_H, because of more calcium adsorption into specifically the phospholipid head region as $CaCl_2$ concentration increases (Figure 3b). This is accompanied by a swelling effect of the bilayer lipid chain zone (d_C changes from 27.5 to 28.0 Å, see Figure 3c). Moreover, the swelling tendency can be linearly fitted with a slope of 0.0074 Å/mM$_{[Ca^{2+}]}$, coinciding with the decreased trend of area per lipid A_l with a slope of −0.0074 Å^2/mM$_{[Ca^{2+}]}$ (Figure 3d). Such consistency suggests a principle conservation of lipid volume in the phospholipid chain stretching in response of calcium adsorption to the lipid head zone of the nanodisc. Presumably, charge interactions between bound calcium ions and the zwitterionic lipid heads inside the nanodisc slightly contracts A_l, leading to a more stretched acyl chains with stronger van der Waals interactions for tighter chain packing. The observed reduction of roughness σ (from 5.5 to 4.7 Å, as shown in Figure 3e) of the phospholipid bilayer is likely a consequence of tighter lipid chain packing. Calcium-induced swelling and tighter packing of vesicle bilayers were both suggested ambiguously in a previous neutron scattering study.[22]

With the adsorbed number of Ca^{2+} obtained from the model-independent result (Table 1) and the model-fitted structural parameters (Table 2), we further derived (detailed in SI) a small hydration number $n_w \approx 2$ (Table 2) for tightly bound water molecules in this hydrophilic zone of lipid headgroup and adsorbed Ca^{2+}. Previous reports[40,41] suggested that there are only a few tightly bound water molecules in the phospholipid head zone, despite that there are a significantly more water molecules (~10) in the vicinity associated weakly with the lipid-head zone.[41] Even with a large enthalpy of hydration (−1577 kJ/mol),[42] calcium could still intervene in the lipid membrane without changing the membrane hydration.

On the basis of the structure and composition information obtained (Tables 1 and 2) for the concentration dependent Ca^{2+} binding to the DMPC nanodisc, a binding isotherm of χ_b versus the free Ca^{2+} concentration C_f (i.e., with the membrane-adsorbed Ca^{2+} concentration subtracted from the total Ca^{2+} concentration) can be established as shown in Figure 4. We further adopt a modified Gouy−Chapman model for electric double layers[43,44] to describe the measured Ca^{2+} binding isotherm. According to the model, the equilibrium χ_b is correlated to C_f via an intrinsic binding constant K in form of

$$\chi_b = KC_f \exp(-ze_oF\psi_0/RT) \quad (4)$$

Table 2. Fitted Parameters of the Elliptical Cylinder SAXS Model Selectively Shown for the DMPC Nanodisc with Different [$CaCl_2$] Present in Buffer at 13 °C[a]

[$CaCl_2$]	0 mM	25 mM	50 mM	75 mM
R (Å)	38.6 ± 0.04	37.5 ± 0.05	37.5 ± 0.04	37.9 ± 0.07
d_C (Å)	27.5 ± 0.07	27.6 ± 0.07	27.8 ± 0.05	28.0 ± 0.09
ρ_C (10^{-6} Å^{-2})	8.63 ± 0.01	8.61 ± 0.01	8.58 ± 0.01	8.56 ± 0.01
ρ_H (10^{-6} Å^{-2})	11.31 ± 0.01	11.44 ± 0.01	11.55 ± 0.01	11.59 ± 0.02
$N_{l,fit}$	187 ± 1[b]	178 ± 1	179 ± 1	183 ± 1
n_w	1.6 ± 0.1	1.6 ± 0.1	1.7 ± 0.1	1.7 ± 0.1
Ψ_0 (mV)		85	92	97

[a] d_H = 9.0 Å, d_{belt} = 8.5 Å, and ρ_{belt} = 10.6 × 10^{-6} Å^{-2} are fixed values in the fitting algorithm. The overall dimensions of the nanodisc without calcium are defined by the height (45.5 Å = d_c + 2d_H), diameter (94.2 Å = 2R + 2d_{belt}), and a fitted aspect ratio ε = 1.0 for a circular shape (Table S-1). The lipid number $N_{l,fit}$ and hydration number n_w are deduced parameters. Ψ_0 is the charge potential deduced based on the modified GC model. [b] The value is of ~10% difference from that in Table 1 because of the approximated model of elliptical cylinder shape used in the SAXS data fitting. The cylinder shell structure may not perfectly describe the MSP conformation surrounding the lipid bilayer.

DOI: 10.1021/acs.jpclett.8b01651
J. Phys. Chem. Lett. 2018, 9, 4287−4293

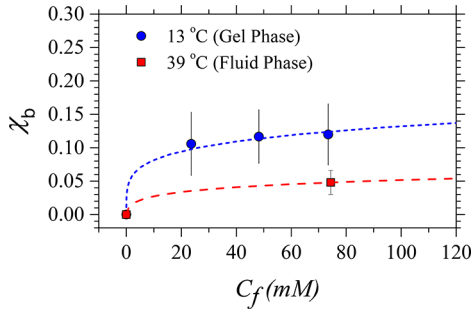

Figure 4. Calcium-to-lipid binding ratio, χ_b, vs free bulk concentration of calcium ion C_f, for the DMPC nanodisc at 13 °C (gel phase) and 39 °C (fluid phase). The data are fitted (dotted and dashed curves) using a modified Gouy−Chapman model.

with the charge number $z = 2$ for calcium ions, units of elementary charge e_0, Faraday constant F, and thermal energy RT.[43,45−47] The charge potential $\Psi_0(\chi_b)$ is built from the adsorbed ions to the membrane, and is regulated by the equilibrium Ca^{2+} concentration immediately above the membrane $C_m = C_f \exp(-zF\Psi_0/RT)$. In the modified GC model, the membrane surface charge density σ reaches equilibrium with the electrolytes in the solution, and

$$\sigma^2 = \sum_i \alpha c_i[\exp(-z_i e_o F\psi_0/RT) - 1)] \quad (5)$$

where $\alpha = 2000\varepsilon_0\varepsilon_R RT$, with ε_0 for the permittivity of free space and ε_R the dielectric constant of water. c_i and z_i are respectively the concentration and charge number of the ith electrolyte (20 mM NaCl in our case) in the bulk aqueous phase. Furthermore, the mean membrane surface charge density may be alternatively approximated by $\sigma = z\chi_b/(A_l + A_{Ca}\chi_b)$, with the average lipid head area $A_l = 49.6$ Å^2 taken from the results of SAXS model fitting (Figure 3d) and an estimated area $A_{Ca} = 3.1$ Å^2 of Ca^{2+}. Therefore, χ_b can be correlated with the modified GC model in the form

$$\chi_b = KC_f[(\beta + 2) + (\beta^2 + 4\beta)^{1/2}]/2]^{-Z} \quad (6)$$

with $\beta = [ze_o\chi_b/(A_L+A_{Ca}X_b)]^2/\alpha c$ (with monovalent electrolyte NaCl, $c = c_i$). For practical data fitting, eq 6 is rearranged into $C_f = (\chi_b/K)[(\beta + 2) + (\beta^2 + 4\beta)^{1/2}]/2]^Z$, which allows convenient data fitting with one single parameter K.

Shown in Figure 4 is the binding isotherm decently described by the modified GC model with $K = 4260 \pm 460$ M^{-1} (corresponding to a change of Gibbs free energy $\Delta G = -29.5$ kJ/mol).[43] It is possible that the previously unclarified two-stage Ca^{2+}-adsorption to a plasma membrane was resulted from two characteristic adsorptions, which are dominated by the membrane proteins (with ∼8 times higher K values and early saturation)[48] and the neutral lipids of the plasma membrane, respectively in low and high calcium concentrations. From the fitted K value, we can further deduce the charge potential $\Psi_0(\chi_b)$ on the nanodisc using eq 4. As listed in Table 2, Ψ_0 saturates to 97 mV with $\chi_b = 0.12$, when the buffer $[CaCl_2]$ increases to 75 mM.

We further conducted similar measurements at 39 °C for the nanodisc of DMPC at the fluid phase, in solutions without and with 75 mM $CaCl_2$ (the gel-to-fluid phase transition temperature of DMPC bilayers is ∼24 °C[49]). The data and correspondingly extracted structures (Figure S-3 and Table S-2) clearly reveal similar Ca-adsorption effects as that observed at 13 °C (the gel phase regime), including membrane swelling and insertion of Ca^{2+} into the headgroup region of the nanodisc bilayers. We note that in the gel-to-fluid phase transition, the zone thickness of the bilayer lipid chains shrinks greatly by 4 Å more, and the nanodisc shape changes from circular to elliptical with an aspect ratio $\varepsilon = 0.82$; whereas the number of lipids in the nanodisc remains relatively stable (cf., Table S1 and Table S2). The calcium-lipid binding ratio, however, drops to $\chi_b = 0.048 \pm 0.018$ (∼40% of that at 13 °C, Table S-2), leading to a drastically reduced $K = 31 \pm 3$ M^{-1} ($\Delta G = -19.4$ kJ/mol) (Figure 4) and a smaller $\Psi_0 = 52$ mV. The lower Ca^{2+}-adsorption χ_b value at the fluid phase of the nanodisc, nevertheless, corresponds to a substantial effective charge capacity of approximately a few $\mu F/cm^2$ in the thin hydrophilic headgroup layer of 10 Å in thickness. This high charge capacity suggests that membranes might act as switched-capacitors for signaling calcium-dependent cellular processes,[50,51] with the charging time constant depending on the temperature-sensitive binding affinity revealed. Possible consequences of the membrane charging via ion adsorption would be forced mechanical vibration of the membrane, reorganization of the lipids, or conformation changes of transmembrane proteins such as voltage-gated channels.[52−54] We, however, note that the physicochemical and dynamic properties of the nanodisc system need to be examined further before applying the current results to real biological membranes containing significant fraction of negatively charged lipids (hence, membrane discharging with adsorption of Ca^{2+}).

In summary, we have developed an integrated analysis scheme to reveal the compositional and structural changes of the DMPC nanodisc upon calcium binding based on integrated measurements of HPLC-SAXS/UV−vis/RI. Our results reveal the detailed structure of the nanodisc and the substantial calcium-lipid binding ratio that leads to delicate nanodisc charging and swelling. The binding isotherm together with the modified GC model allows extracting the intrinsic binding constant and leaflet potential for the Ca^{2+}-adsorbed nanodisc. The substantial calcium-lipid binding ratio and leaflet potential of the Ca^{2+}-nanodisc complex at the fluid phase support a possible signaling pathway via direct calcium-membrane interactions. Our developed methodology would greatly promote the use of highly monodisperse and stable nanodiscs as a promising membrane platform for studying structural changes and composition reconstitution of membranes upon incorporation of membrane proteins or small ions.

■ ASSOCIATED CONTENT

Supporting Information

The Supporting Information is available free of charge on the ACS Publications website at DOI: 10.1021/acs.jpclett.8b01651.

Materials and experimental methods; SAXS data and data analysis; and fitting results and parameters (PDF)

Number of absorbents on nanodiscs using absolute intensities of SAXS, UV−vis absorption, and refractive index (XLSX)

■ AUTHOR INFORMATION

Corresponding Authors

*Tel: +886-2-2366-8210. E-mail: tyyu@pub.iams.sinica.edu.tw.

DOI: 10.1021/acs.jpclett.8b01651
J. Phys. Chem. Lett. 2018, 9, 4287−4293

*Tel: +886-3-578-0281, ext 7108. Fax: +886-3-578-3813. E-mail: usjeng@nsrrc.org.tw.

ORCID

Orion Shih: 0000-0002-0610-6856
Yi-Qi Yeh: 0000-0002-2387-3600
Tsyr-Yan Yu: 0000-0001-7051-4769
U-Ser Jeng: 0000-0002-2247-5061

Notes

The authors declare no competing financial interest.

■ ACKNOWLEDGMENTS

This work benefited from the use of the SasView application, originally developed under NSF award DMR-0520547. SasView contains code developed with funding from the European Union's Horizon 2020 research and innovation programme under the SINE2020 project, grant agreement No 654000. Funding support of Minister of Science and Technology, Taiwan (under MOST 105-2112-M-213-010-MY3, 105-2113-M-001-021-MY2 and 106-2627-M-213-001) is acknowledged.

■ REFERENCES

(1) Rossi, C.; Homand, J.; Bauche, C.; Hamdi, H.; Ladant, D.; Chopineau, J. Differential Mechanisms for Calcium-Dependent Protein/Membrane Association as Evidenced from SPR-Binding Studies on Supported Biomimetic Membranes. *Biochemistry* **2003**, *42*, 15273−15283.

(2) Berridge, M. J.; Lipp, P.; Bootman, M. D. The Versatility and Universality of Calcium Signalling. *Nat. Rev. Mol. Cell Biol.* **2000**, *1*, 11−21.

(3) Portis, A.; Newton, C.; Pangborn, W.; Papahadjopoulos, D. Studies on the Mechanism of Membrane Fusion: Evidence for an Intermembrane Calcium(2+) Ion-Phospholipid Complex, Synergism with Magnesium(2+) Ion, and Inhibition by Spectrin. *Biochemistry* **1979**, *18*, 780−790.

(4) Weisthal, S.; Keinan, N.; Ben-Hail, D.; Arif, T.; Shoshan-Barmatz, V. Ca(2+)-Mediated Regulation of VDAC1 Expression Levels is Associated with Cell Death Induction. *Biochim. Biophys. Acta, Mol. Cell Res.* **2014**, *1843*, 2270−2281.

(5) Glancy, B.; Balaban, R. S. Role of Mitochondrial Ca2+ in the Regulation of Cellular Energetics. *Biochemistry* **2012**, *51*, 2959−2973.

(6) Oshima, H.; Inoko, Y.; Mitsui, T. Hamaker Constant and Binding Constants of Ca^{2+} and Mg^{2+} in Dipalmitoyl Phosphatidylcholine/Water System. *J. Colloid Interface Sci.* **1982**, *86*, 57−72.

(7) Newton, C.; Pangborn, W.; Nir, S.; Papahadjopoulos, D. Specificity of Ca^{2+} and Mg^{2+} Binding to Phosphatidylserine Vesicles and Resultant Phase Changes of Bilayer Membrane Structure. *Biochim. Biophys. Acta, Biomembr.* **1978**, *506*, 281−287.

(8) Coorssen, J. R.; Rand, R. P. Structural Effects of Neutral Lipids on Divalent Cation-Induced Interactions of Phosphatidylserine-Containing Bilayers. *Biophys. J.* **1995**, *68*, 1009−1018.

(9) Feigenson, G. W. Calcium Ion Binding between Lipid Bilayers: the Four-Component System of Phosphatidylserine, Phosphatidylcholine, Calcium Chloride, and Water. *Biochemistry* **1989**, *28*, 1270−1278.

(10) Huster, D.; Arnold, K.; Gawrisch, K. Strength of Ca^{2+} Binding to Retinal Lipid Membranes: Consequences for Lipid Organization. *Biophys. J.* **2000**, *78*, 3011−3018.

(11) Roux, M.; Bloom, M. Calcium, Magnesium, Lithium, Sodium, and Potassium Distributions in the Headgroup Region of Binary Membranes of Phosphatidylcholine and Phosphatidylserine as Seen by Deuterium NMR. *Biochemistry* **1990**, *29*, 7077−7089.

(12) Akutsu, H.; Seelig, J. Interaction of Metal Ions with Phosphatidylcholine Bilayer Membranes. *Biochemistry* **1981**, *20*, 7366−7373.

(13) Lehrmann, R.; Seelig, J. Adsorption of Ca^{2+} And La^{3+} to Bilayer Membranes: Measurement of the Adsorption Enthalpy and Binding Constant with Titration Calorimetry. *Biochim. Biophys. Acta, Biomembr.* **1994**, *1189*, 89−95.

(14) Jacobson, K.; Papahadjopoulos, D. Phase Transitions and Phase Separations in Phospholipid Membranes Induced by Changes in Temperature, pH, and Concentration of Bivalent Cations. *Biochemistry* **1975**, *14*, 152−161.

(15) Silvius, J. R.; Gagne, J. Calcium-Induced Fusion and Lateral Phase Separations in Phosphatidylcholine-Phosphatidylserine Vesicles. Correlation by Calorimetric and Fusion Measurements. *Biochemistry* **1984**, *23*, 3241−3247.

(16) Binder, H.; Zschörnig, O. The Effect of Metal Cations on the Phase Behavior and Hydration Characteristics of Phospholipid Membranes. *Chem. Phys. Lipids* **2002**, *115*, 39−61.

(17) Martin-Molina, A.; Rodriguez-Beas, C.; Faraudo, J. Effect of Calcium and Magnesium on Phosphatidylserine Membranes: Experiments and All-Atomic Simulations. *Biophys. J.* **2012**, *102*, 2095−2103.

(18) Melcrova, A.; Pokorna, S.; Pullanchery, S.; Kohagen, M.; Jurkiewicz, P.; Hof, M.; Jungwirth, P.; Cremer, P. S.; Cwiklik, L. The Complex Nature of Calcium Cation Interactions with Phospholipid Bilayers. *Sci. Rep.* **2016**, *6*, 38035.

(19) Averbakh, A.; Lobyshev, V. I. Adsorption of Polyvalent Cations to Bilayer Membranes from Negatively Charged Lipid: Estimating the Lipid Accessibility in the Case of Complete Binding. *J. Biochem. Biophys. Methods* **2000**, *45*, 23−44.

(20) Satoh, K. Determination of Binding Constants of Ca^{2+}, Na^{+}, And Cl^{-} Ions to Liposomal Membranes of Dipalmitoylphosphatidylcholine at Gel Phase by Particle Electrophoresis. *Biochim. Biophys. Acta, Biomembr.* **1995**, *1239*, 239−248.

(21) McLaughlin, S. Adsorption of Divalent Cations to Bilayer Membranes Containing Phosphatidylserine. *J. Gen. Physiol.* **1981**, *77*, 445−473.

(22) Uhrikova, D.; Kucerka, N.; Teixeira, J.; Gordeliy, V.; Balgavy, P. Structural Changes in Dipalmitoylphosphatidylcholine Bilayer Promoted by Ca^{2+} Ions: a Small-Angle Neutron Scattering Study. *Chem. Phys. Lipids* **2008**, *155*, 80−89.

(23) Sinn, C. G.; Antonietti, M.; Dimova, R. Binding of Calcium to Phosphatidylcholine−Phosphatidylserine Membranes. *Colloids Surf., A* **2006**, *282*−*283*, 410−419.

(24) Denisov, I. G.; Sligar, S. G. Nanodiscs for Structural and Functional Studies of Membrane Proteins. *Nat. Struct. Mol. Biol.* **2016**, *23*, 481−486.

(25) Bayburt, T. H.; Grinkova, Y. V.; Sligar, S. G. Self-Assembly of Discoidal Phospholipid Bilayer Nanoparticles with Membrane Scaffold Proteins. *Nano Lett.* **2002**, *2*, 853−856.

(26) Denisov, I. G.; Grinkova, Y. V.; Lazarides, A. A.; Sligar, S. G. Directed Self-Assembly of Monodisperse Phospholipid Bilayer Nanodiscs with Controlled Size. *J. Am. Chem. Soc.* **2004**, *126*, 3477−3487.

(27) Nasr, M. L.; Baptista, D.; Strauss, M.; Sun, Z. J.; Grigoriu, S.; Huser, S.; Pluckthun, A.; Hagn, F.; Walz, T.; Hogle, J. M.; Wagner, G. Covalently Circularized Nanodiscs for Studying Membrane Proteins and Viral Entry. *Nat. Methods* **2017**, *14*, 49−52.

(28) Raschle, T.; Hiller, S.; Yu, T.-Y.; Rice, A. J.; Walz, T.; Wagner, G. Structural and Functional Characterization of the Integral Membrane Protein VDAC-1 in Lipid Bilayer Nanodiscs. *J. Am. Chem. Soc.* **2009**, *131*, 17777−17779.

(29) Berthaud, A.; Manzi, J.; Pérez, J.; Mangenot, S. Modeling Detergent Organization around Aquaporin-0 Using Small-Angle X-Ray Scattering. *J. Am. Chem. Soc.* **2012**, *134*, 10080−10088.

(30) Yeh, Y.-Q.; Liao, K.-F.; Shih, O.; Shiu, Y.-J.; Wu, W.-R.; Su, C.-J.; Lin, P.-C.; Jeng, U.-S. Probing the Acid-Induced Packing Structure Changes of the Molten Globule Domains of a Protein near Equilibrium Unfolding. *J. Phys. Chem. Lett.* **2017**, *8*, 470−477.

(31) Shih, O.; Yeh, Y.-Q.; Liao, K.-F.; Sung, T.-C.; Chiang, Y.-W.; Jeng, U.-S. Oligomerization Process of Bcl-2 Associated X Protein Revealed from Intermediate Structures in Solution. *Phys. Chem. Chem. Phys.* **2017**, *19*, 7947−7954.

DOI: 10.1021/acs.jpclett.8b01651
J. Phys. Chem. Lett. 2018, 9, 4287−4293

(32) Svergun, D. I. Determination of the Regularization Parameter in Indirect-Transform Methods Using Perceptual Criteria. *J. Appl. Crystallogr.* **1992**, *25*, 495−503.
(33) Bernadó, P.; Mylonas, E.; Petoukhov, M. V.; Blackledge, M.; Svergun, D. I. Structural Characterization of Flexible Proteins Using Small-Angle X-Ray Scattering. *J. Am. Chem. Soc.* **2007**, *129*, 5656−5664.
(34) Skar-Gislinge, N.; Kynde, S. A.; Denisov, I. G.; Ye, X.; Lenov, I.; Sligar, S. G.; Arleth, L. Small-Angle Scattering Determination of the Shape and Localization of Human Cytochrome P450 Embedded in a Phospholipid Nanodisc Environment. *Acta Crystallogr., Sect. D: Biol. Crystallogr.* **2015**, *71*, 2412−2421.
(35) Skar-Gislinge, N.; Arleth, L. Small-Angle Scattering from Phospholipid Nanodiscs: Derivation and Refinement of a Molecular Constrained Analytical Model Form Factor. *Phys. Chem. Chem. Phys.* **2011**, *13*, 3161−3170.
(36) Skar-Gislinge, N.; Simonsen, J. B.; Mortensen, K.; Feidenhans'l, R.; Sligar, S. G.; Lindberg Møller, B.; Bjørnholm, T.; Arleth, L. Elliptical Structure of Phospholipid Bilayer Nanodiscs Encapsulated by Scaffold Proteins: Casting the Roles of the Lipids and the Protein. *J. Am. Chem. Soc.* **2010**, *132*, 13713−13722.
(37) Rizzuto, R.; De Stefani, D.; Raffaello, A.; Mammucari, C. Mitochondria as Sensors and Regulators of Calcium Signalling. *Nat. Rev. Mol. Cell Biol.* **2012**, *13*, 566−578.
(38) Bathori, G.; Csordas, G.; Garcia-Perez, C.; Davies, E.; Hajnoczky, G. Ca^{2+}-Dependent Control of the Permeability Properties of the Mitochondrial Outer Membrane and Voltage-Dependent Anion-Selective Channel (VDAC). *J. Biol. Chem.* **2006**, *281*, 17347−17358.
(39) Guinier, A. La Diffraction des Rayons X aux Tres Petits Angles; Application a L'etude de Phenomenes Ultramicroscopiques. *Ann. Phys.* **1939**, *11*, 161−237.
(40) Graziano, V.; Miller, L.; Yang, L. Interpretation of Solution Scattering Data from Lipid Nanodiscs. *J. Appl. Crystallogr.* **2018**, *51*, 157−166.
(41) Yamada, T.; Takahashi, N.; Tominaga, T.; Takata, S. I.; Seto, H. Dynamical Behavior of Hydration Water Molecules between Phospholipid Membranes. *J. Phys. Chem. B* **2017**, *121*, 8322−8329.
(42) Smith, D. W. Ionic Hydration Enthalpies. *J. Chem. Educ.* **1977**, *54*, 540−542.
(43) Seelig, J. Thermodynamics of Lipid-Peptide Interactions. *Biochim. Biophys. Acta, Biomembr.* **2004**, *1666*, 40−50.
(44) Kinraide, T. B. Use of a Gouy-Chapman-Stern Model for Membrane-Surface Electrical Potential to Interpret Some Features of Mineral Rhizotoxicity. *Plant Physiol.* **1994**, *106*, 1583−1592.
(45) Su, C. J.; Wu, S. S.; Jeng, U. S.; Lee, M. T.; Su, A. C.; Liao, K. F.; Lin, W. Y.; Huang, Y. S.; Chen, C. Y. Peptide-Induced Bilayer Thinning Structure of Unilamellar Vesicles and the Related Binding Behavior as Revealed by X-Ray Scattering. *Biochim. Biophys. Acta, Biomembr.* **2013**, *1828*, 528−534.
(46) Stankowski, S. Surface Charging by Large Multivalent Molecules. Extending the Standard Gouy-Chapman Treatment. *Biophys. J.* **1991**, *60*, 341−351.
(47) Beschiaschvili, G.; Seelig, J. Peptide Binding to Lipid Bilayers. Nonclassical Hydrophobic Effect and Membrane-Induced pK Shifts. *Biochemistry* **1992**, *31*, 10044−10053.
(48) Peterson, R. N.; Russell, L.; Bundman, D.; Freund, M. Calcium Binding to Plasma Membrane Vesicles of Boar Spermatozoa. *Biol. Reprod.* **1979**, *21*, 583−588.
(49) Kucerka, N.; Liu, Y.; Chu, N.; Petrache, H. I.; Tristram-Nagle, S.; Nagle, J. F. Structure of Fully Hydrated Fluid Phase DMPC and DLPC Lipid Bilayers Using X-Ray Scattering from Oriented Multilamellar Arrays and from Unilamellar Vesicles. *Biophys. J.* **2005**, *88*, 2626−2637.
(50) Simms, B. A.; Zamponi, G. W. Neuronal Voltage-Gated Calcium Channels: Structure, Function, and Dysfunction. *Neuron* **2014**, *82*, 24−45.
(51) Eijkelkamp, N.; Linley, J. E.; Baker, M. D.; Minett, M. S.; Cregg, R.; Werdehausen, R.; Rugiero, F.; Wood, J. N. Neurological Perspectives on Voltage-Gated Sodium Channels. *Brain* **2012**, *135*, 2585−2612.
(52) Rapizzi, E.; Pinton, P.; Szabadkai, G.; Wieckowski, M. R.; Vandecasteele, G.; Baird, G.; Tuft, R. A.; Fogarty, K. E.; Rizzuto, R. Recombinant Expression of the Voltage-Dependent Anion Channel Enhances the Transfer of Ca^{2+} Microdomains to Mitochondria. *J. Cell Biol.* **2002**, *159*, 613−624.
(53) Keinan, N.; Pahima, H.; Ben-Hail, D.; Shoshan-Barmatz, V. The Role of Calcium in VDAC1 Oligomerization and Mitochondria-Mediated Apoptosis. *Biochim. Biophys. Acta, Mol. Cell Res.* **2013**, *1833*, 1745−1754.
(54) Tan, W.; Colombini, M. VDAC Closure Increases Calcium Ion Flux. *Biochim. Biophys. Acta, Biomembr.* **2007**, *1768*, 2510−2515.

DOI: 10.1021/acs.jpclett.8b01651
J. Phys. Chem. Lett. 2018, 9, 4287−4293